Journal of Catalysis 354 (2017) 113–127

Contents lists available at ScienceDirect

Journal of Catalysis

journal homepage: www.elsevier.com/locate/jcat

NHC-stabilised Rh nanoparticles: Surface study and application in the catalytic hydrogenation of aromatic substrates

Francisco Martinez-Espinar [a,c], Pascal Blondeau [d], Pau Nolis [e], Bruno Chaudret [c], Carmen Claver [a,b], Sergio Castillón [a,b,*], Cyril Godard [a,b,*]

[a] Departament de Química Física i Inorgànica, Universitat Rovira i Virgili, Marcel.li Domingo s/n, 43007 Tarragona, Spain
[b] Centre Tecnològic de Química, C/ Marcel.li Domingo s/n, 43007 Tarragona, Spain
[c] Laboratoire de Physique et Chimie de Nano-Objets, Université de Toulouse, CNRS, INSA, UPS, 135 Avenue de Rangueil, 31077 Toulouse, France
[d] Departament de Química Analítica i Orgànica, Universitat Rovira i Virgili, C/ Marcel.li Domingo s/n, 43007 Tarragona, Spain
[e] Universitat Autonoma de Barcelona, Servei de Ressonància Magnètica Nuclear, Edifici C – Campus UAB, 08193 Cerdanyola del Vallés, Barcelona, Spain

ARTICLE INFO

Article history:
Received 15 March 2017
Revised 28 July 2017
Accepted 9 August 2017

Keywords:
Rhodium
Nanoparticles
NHC
Surface
Hydrogenation
Phenol
Pyridine
Aromatic ketone
Quinoline

ABSTRACT

New Rh-NPs stabilised by N-Heterocyclic Carbenes (NHC) were synthesized by decomposition of [Rh(η^3-C_3H_5)$_3$] under H_2 atmosphere and fully characterized. Surface studies by FT-IR and NMR spectroscopy employing isotopically labelled ligands were also performed. The **Rh$^{0.2}$** NPs are active catalysts in the reduction of various aromatic substrates. In the reduction of phenol, high selectivities to cyclohexanone or cyclohexanol were obtained depending on the reaction conditions. However, this catalytic system exhibited much lower activity in the hydrogenation of substituted phenols. Pyridine was easily hydrogenated under mild conditions and interestingly, the hydrogenation of 4-methyl and 4-trifluoromethylpyridine resulted slower than that of 2-methylpyridine. The hydrogenation of 1-(pyridin-2-yl)propan-2-one provided the β-enaminone **13a** in high yield as a consequence of the partial reduction of the pyridine ring followed by isomerization. Quinoline could be either partially hydrogenated to 1,2,3,4-tetrahydroquinoline or fully reduced to decahydroquinoline by adjusting the reaction conditions.

1. Introduction

Over the last decades, transition metal-nanoparticles (M-NPs) have received a great deal of attention as catalysts since they potentially combine the advantages of heterogeneous and homogeneous catalysts, exhibiting high activities while retaining tunability and selectivity through their well defined composition with narrow size distribution [1–3]. Moreover, they catalyse reactions in which molecular systems are less active or inactive, such as arene reduction [4–9] and aldehyde reduction in α,β-unsaturated aldehydes [10].

The stabilisation of M-NPs can be realised in the presence of polymers, surfactants or ligands, which allows the control of their size, shape and dispersion as well as their surface state. The choice of an appropriate stabiliser for the M-NPs is thus of critical importance in tailoring their properties and consequently their catalytic performance [11]. The influence of various ligands has been recently examined by several research groups and significant efforts have been made in the synthesis of ligand-stabilised nanoparticles to achieve control of their properties [12]. Recently, NHC carbenes revealed as excellent stabilisers for Ru [13–16], Pd [17,18] Pt [19,20] and Au [21–24] NPs due to their strong coordination properties. Moreover, these NHC-stabilised nanocatalysts revealed efficient in the hydrogenation of several types of substrates such as aromatic ketones and nitroarenes. However, no Rh-NPs stabilised by NHC-ligands have been reported to date and it was therefore thought that the synthesis of such systems and their application in hydrogenation reactions would be of interest.

The hydrogenation of aromatics is of great interest from both academic and industrial points of view with energy and environmental issues of current importance. For instance, the hydrogenation of phenol and derivatives is an important process in industrial organic chemistry and these substrates are often used as models for lignin fragments [25–29]. The catalytic hydrogenation of phenol is also of commercial and environmental significance for the

* Corresponding authors at: Universitat Rovira i Virgili, C/ Marcel.li Domingo s/n, 43007 Tarragona, Spain, and Centre Tecnològic de Química, C/Marcel.li Domingo s/n, 43007 Tarragona, Spain.
E-mail addresses: chaudret@insa-toulouse.fr (B. Chaudret), sergio.castillon@urv.cat (S. Castillón), cyril.godard@urv.cat (C. Godard).

http://dx.doi.org/10.1016/j.jcat.2017.08.010
0021-9517/

formation of cyclohexanone and cyclohexanol, which is the primary stage for the production of adipic acid and caprolactam [30] used for the production of Nylon 6 and Nylon 66 [31] (Scheme 1).

Various metal NPs have been used as catalysts in the phenol reduction. In this process, RhNPs usually mainly provide cyclohexanol [32], although their activity can be modulated by the use of the appropriate support and reaction conditions. For instance, when RhNPs supported on MOFs [33] and ILs [34] are used as catalysts at low temperatures and/or H_2 pressures, selectivities up to 99% to cyclohexanone were achieved. A few reports describe the use of IrNPs to produce cylcohexanol [35]. In contrast, PdNPs provides cyclohexanone with high selectivity independently of the support [36].

The hydrogenation of N-heteroaromatics is also of high interest for the purification of heavy and extra heavy oils and bitumens, which are likely to become the refinery feeds in the future due to the foreseen shortage of light fuels reserves. The reduction of such compounds was mainly reported employing Rh and Ru-based catalytic systems. In the presence of RhNPs based catalysts, the hydrogenation of pyridine [37–42] 2-picoline [37,40,43] 4-picoline [40] and 3-hydroxypyridine [44] has been reported using H_2 pressures in the range 1–10 bar. The diastereoselective reduction of pyridine analogues bearing an amine group such as substituted-4-aminopyridines, was also reported using Rh/C as catalyst [45]. In this reaction, the protection of the amine with an electron-withdrawing group was necessary for the reaction to proceed. Ru NPs stabilised by NHC ligands [46] and Phosphine-functionalized Ionic Liquids (PFILs) [47] were used in the reduction of 2- and 3-acetylpyridines, affording mainly the selective reduction of the keto group in organic solvents while full reduction was reached in water [47]. Ru NPs supported on magnesium oxide were also reported as dual-site catalysts in the reduction of N-heteroaromatics such as pyridine and other polycyclic compounds [48]. These NPs exhibited high activity for a broad range of aromatic substrates and excellent recyclability.

Among these substrates, the hydrogenation of quinoline and derivatives is of particular interest since the decahydroquinoline (DHQ) skeleton, formed by full reduction of these compounds, is widely employed in the synthesis of petrochemicals [49], fine chemicals and pharmaceuticals [50]. Although this process has been extensively studied, the catalytic reduction of this class of compounds remains nowadays a challenge. The reaction proceeds in two steps: quinoline is first hydrogenated to 1,2,3,4-tetrahydroquinoline (^{1}THQ) by reduction of the pyridine ring, or to 5,6,7,8-tetrahydroquinoline (^{5}THQ) by reduction of the arene ring and, subsequently, these intermediates are reduced to form DHQ. In general, the pyridine ring is preferably reduced although various degrees of selectivity have been described [48,39,40,43,47,51,77]. Complete reduction of both rings has only been described using colloidal [37,47] and supported [52] Ru NPs and supported Rh NPs [53], however high temperatures (>100 °C) and/or high H_2 pressures (>50 bar) to reach full reduction of quinoline.

Here, we report the synthesis and characterisation of novel RhNPs stabilised by N-heterocyclic carbenes (NHCs) and their application as efficient catalysts in the hydrogenation under mild conditions of aromatic ketones, phenols and N-heteroaromatic substrates, including quinoline.

2. Results and discussion

2.1. Synthesis and characterization of the catalyst

The rhodium nanoparticles described in this work were synthesized by decomposition of [Rh(η^3-C_3H_5)$_3$] in THF at 35 °C under 4 bar of H_2 in the presence of substoichiometric amounts of the 1,3-bis(2,6-diisopropylphenyl)imidazol-2-ylidene (IPr) NHC ligand **L** (Scheme 2). This synthetic methodology allows the formation of clean-surface nanoparticles, which is necessary for surface studies and for undertaking reproducible chemistry [54]. The ligand to Rh ratio was varied from 0.2 to 0.6 during the synthesis.

Transmission Electron Microscopy (TEM) revealed the formation of small and well-dispersed RhNPs of mean diameters of 1.68 ± 0.26 nm (**Rh$^{0.2}$**), 1.26 ± 0.25 nm (**Rh$^{0.4}$**) and 1.29 ± 0.21 nm (**Rh$^{0.6}$**), exhibiting in all cases spherical shapes and narrow size distributions (Fig. 1). The slight decrease in size at higher ligand concentrations is in agreement with results previously reported for Ru [12]. High Resolution Transmission Electron Microscopy (HRTEM) showed the highly crystalline character of these RhNPs exhibiting a *fcc* packing (Fig. 2). This result was confirmed by the analysis of solid samples by X-ray Diffraction (XRD) and Wide-Angle X-ray

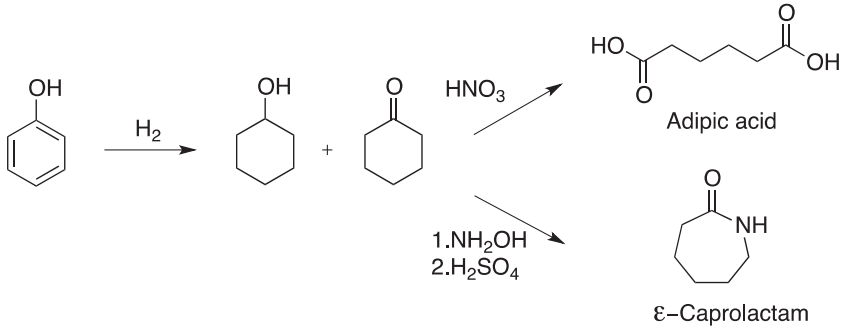

Scheme 1. Adipic acid and ε-caprolactam formation from cyclohexanone, produced by reduction of phenol.

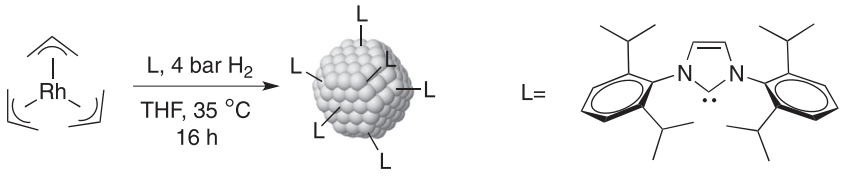

Scheme 2. Synthesis of Rh NPs stabilised by IPr-NHC ligand L.

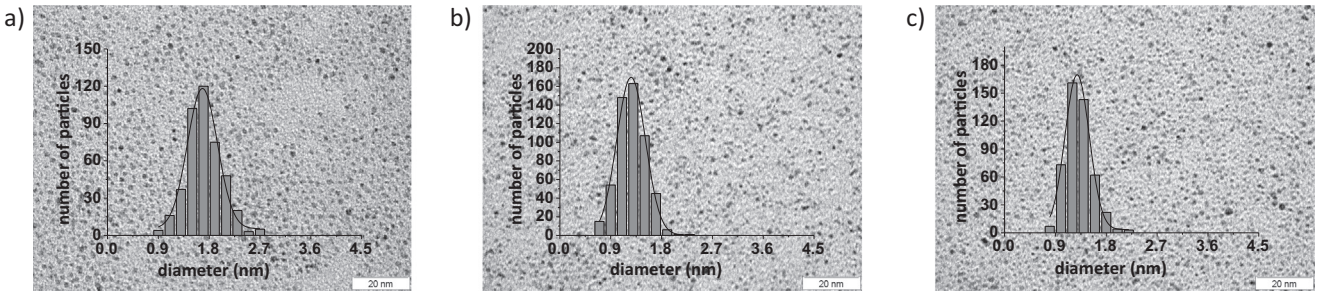

Fig. 1. TEM images of (a) $Rh^{0.2}$, (b) $Rh^{0.4}$, (c) $Rh^{0.6}$.

Scattering (WAXS). No oxidation of these NPs was detected by WAXS and over 97% of Rh^0 was measured at the NPs surface for all samples by X-ray photoelectron spectroscopy (XPS) (see Supporting Information).

The amount of NHC ligand present at the surface of the isolated RhNPs **$Rh^{0.2}$**–**$Rh^{0.6}$** was quantified using thermogravimetric analysis (TGA) (Fig. 3). In all cases, a main weight loss attributed to the decomposition of the **L** ligand was observed between 150 and 400 °C, with values of 21.5, 37 and 36.1 wt% for **$Rh^{0.2}$**, **$Rh^{0.4}$** and **$Rh^{0.6}$**, respectively. Moreover, a weight loss at lower temperature (<150 °C) was also observed and attributed to the loss of coordinated THF. The increase in ligand coverage between **$Rh^{0.2}$** and **$Rh^{0.4}$** is in agreement with the amounts of **L** used during the synthesis of these NPs. In the case of **$Rh^{0.4}$** and **$Rh^{0.6}$** which exhibit similar sizes, comparable values were obtained. This result can be explained by the saturation of the Rh surface when the [**L**]/[Rh] molar ratio is >0.4. At higher ratio, no further ligands can therefore coordinate at the surface of these NPs.

The presence of surface hydrides [55] was quantified by titration using a method reported by some of us [56,57], using 2-norbornene in the absence of added H_2. Values of 0.58, 0.39 and 0.34H/Rh_s were obtained for **$Rh^{0.2}$**, **$Rh^{0.4}$** and **$Rh^{0.6}$** respectively. These values are lower than those reported for RhNPs stabilised by P-based ligands [58] and RuNPs stabilised by PVP and DPPB (between 1.1 and 1.5H/Ru) [59,60] and by the **L** ligand (2.5H/Ru) [13].

The NPs **$Rh^{0.4}$** were also characterised by Infrared spectroscopy and the spectrum compared to that of the IPr ligand (see Figure S16 in the Supporting Information). A main set of signals was observed was detected at 2850–2960 cm^{-1} and attributed to alkyl C-H stretching of the IPr ligand. At lower frequencies, small bands at 1500–1700 cm^{-1} and 680–860 cm^{-1} attributed to the different vibrations of the aromatic rings, were detected. These data confirmed the presence of aromatic moieties from the IPr ligand.

The availability of sites on the NPs surface was studied by Infrared spectroscopy after exposure to 1 bar of CO of **$Rh^{0.2}$**, **$Rh^{0.4}$** and **$Rh^{0.6}$** in the solid state (Scheme 3). In all cases, three different CO stretching frequencies between 2200 and 1700 cm^{-1} were detected and attributed to geminal-terminal (or multicarbonyl) "$Rh(CO)_2$" units (2067 and 2008 cm^{-1}), terminal CO (1995 cm^{-1}) and bridging CO (broad band centred at 1845 cm^{-1}) based on previously reported results [58].

In the case of **$Rh^{0.2}$**, a more intense band for bridging COs was observed compared to the other colloids **$Rh^{0.4}$** and **$Rh^{0.6}$**, indicating a greater availability of the faces of these NPs (Fig. 4). It can therefore be concluded that at low ligand concentration, the ligand mainly coordinates on the edges and apexes of the NPs, and that when an excess of ligand is used, some of the NHC ligands coordinate on the NP faces, in agreement with reports on RuNPs stabilised by the same ligand [13]. Moreover, more geminal "$Rh(CO)_2$" sites were detected when higher amounts of the ligand where used in the synthesis of the NPs (**$Rh^{0.6}$** compared to **$Rh^{0.2}$**), as previously observed by similar Rh systems stabilised by PPh_3 [58].

To explore the effect of CO pressure, the **$Rh^{0.4}$** NPs were exposed to 30 bar of CO. An increase in the bands corresponding to geminal "$Rh(CO)_2$" units located at *ca.* 2070 and 2020 cm^{-1} was observed while no relevant changes were detected for the bands corresponding to terminal and bridging COs (Fig. 4, dashed line). This increase

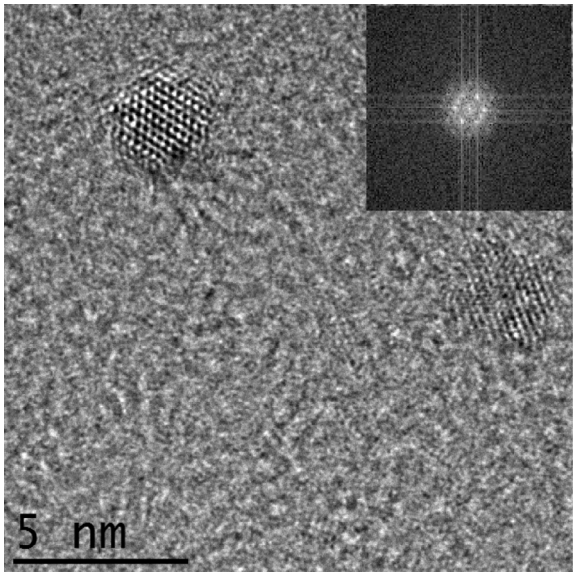

Fig. 2. HRTEM image of $Rh^{0.2}$.

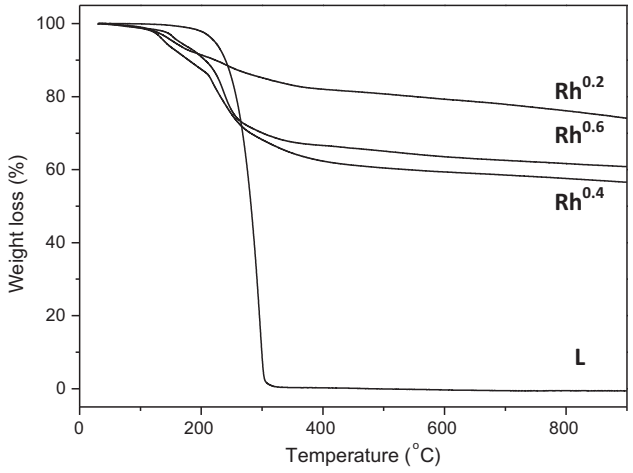

Fig. 3. TGA curves of L and $Rh^{0.2}$, $Rh^{0.4}$ and $Rh^{0.6}$.

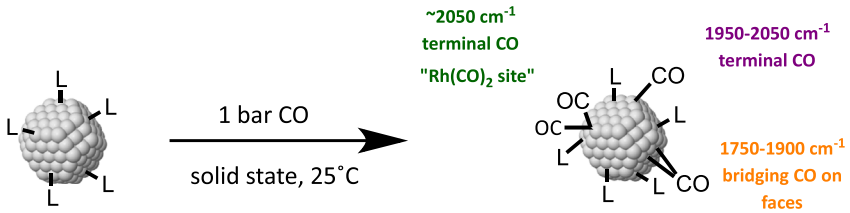

Scheme 3. Representation of CO adsorption onto metallic NPs.

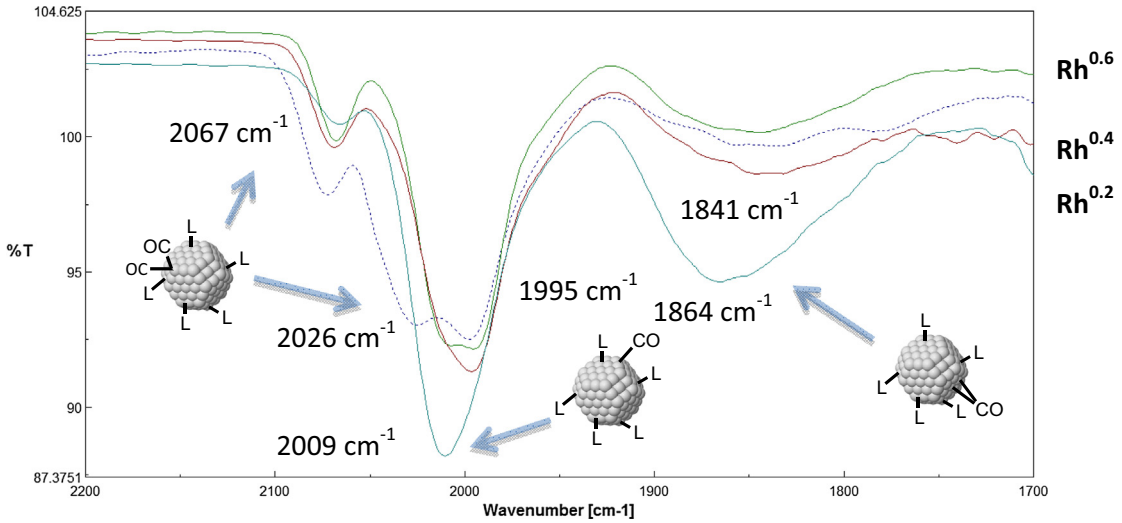

Fig. 4. IR spectra of $Rh^{0.2}$, $Rh^{0.4}$ and $Rh^{0.6}$ after exposure to 1 bar of CO and $Rh^{0.4}$ after exposure to 30 bar of CO (dashed line).

in the amount of "$Rh(CO)_2$" groups on the NPs surface indicated that the coordination of a second CO on coordinatively unsaturated Rh centres depend on the CO pressure.

Solution NMR spectroscopy is not commonly used for the characterization of colloids due to the width of the signals (if observable) from molecules close to the NPs surface as a result of slow molecular tumbling, presence of different chemical environments and magnetic effects as the Knight shift [61]. However, sharp signals have been reported when solution NMR spectra have been recorded in the case of PdNPs [62,63].

A solution NMR study was performed after dissolution of the NPs into THF-d_8. In the ^{1}H NMR spectrum of **$Rh^{0.4}$** at room temperature, a broad signal between 6.75 and 7.75 ppm was observed and attributed to the —CH_{arom}— of the phenyl rings of the coordinated ligand (Fig. S24, Supporting information). Moreover, one signal at 7.94 ppm assigned to the protons of the imidazole backbone and two pairs of "doublets" centred at 0.82 and 1.29 ppm that could be attributed to the —CH_3 of the isopropyl groups were also detected. Other broad signals detected at low chemical shifts (0.5–2 ppm) were observed and could arise from aliphatic protons due to hydrogenation of the **L** ligand, as previously reported in the case of RuNPs stabilised by this ligand [13]. Interestingly, the signals corresponding to the —CH-group of the isopropyl substituents could not be detected. The absence of signals from a ligand is characteristic when placed in close proximity to the NPs surface due to fast T_2 relaxation [64–66]. Interestingly, a broad signal with low intensity corresponding to acidic protons was also observed at 10.23 ppm. This observation indicated the presence of protonated ligands in the surrounding of these NPs. However, the detection of this signal under these conditions also suggests that the protonated ligand is not directly coordinated to the metal surface and is presumably present in the second coordination sphere of the NPs.

The presence of the **L-H$^+$** species was confirmed by the following information extracted from NMR spectrum of RhNPs (**^{13}C-$Rh^{0.4}$**) stabilised by $^{13}C_2$-labelled NHC ligand **L**: (a) the acidic signal at 10.23 ppm exhibited a large ^{13}C-^{1}H coupling (Fig. S25, Supporting information); (b) the presence of two main signals centred at *ca.* 170 and 140 ppm in the $^{13}C\{^1H\}$ NMR spectrum (Fig. S26, Supporting information), characteristic of the C2 carbon atom of metal coordinated NHC-IPr ligand and of the corresponding imidazolium salt, respectively; (c) 2D HSQC ^{1}H-^{13}C that showed the correlation between the carbon signal at 140 ppm with the proton signal previously detected at 7.94 ppm (Fig. S27, Supporting information). These facts confirm that these NPs contained both the NHC carbene **L** and its protonated equivalent **L-H$^+$**.

To obtain additional information on the role of these two species (**L** and **L-H$^+$**) two experiments were performed with **$Rh^{0.4}$**: (a) washing with H_2O, and (b) reacting with PPh_3 and $P(OPh)_3$. No variations in the ^{1}H and ^{13}C NMR spectra were observed in both cases, indicating that both species are contained in the nanoparticle environment [21,67].

Looking for additional information about the stability of ligand coordination, the same sample containing **^{13}C-$Rh^{0.4}$** in THF-d_8 was exposed to 30 bar of CO using a sapphire high pressure NMR tube and ^{1}H and $^{13}C\{^1H\}$ NMR spectra were recorded. In the ^{1}H NMR (Fig. S29, Supporting information), a series of new sharp signals at 9.27 ppm (doublet, coupling with ^{13}C labelled carbon, note that the acidic signal appeared previously at 10.23 ppm), 7.1–7.7 ppm (aromatic protons), 1.1–1.3 ppm (doublet, -CH_3), and 2.81 ppm (multiplet, —CH—, not observed previously), were attributed to protonated IPr ligands not located in the nanoparticle environment. Besides, a new doublet resonance ($J_{Rh\text{-}C}$ = 46.5 Hz) centred at 180.84 ppm was detected in the $^{13}C\{^1H\}$ NMR under these conditions (Fig. S30, Supporting information). This latter signal was assigned to a molecular Rh(I)-L complex formed by leaching from

the NPs surface under CO pressure based on literature values [68]. This experiment therefore demonstrated that under high CO pressure the protonated ligand **L-H$^+$** is released and that a molecular Rh-NHC species is formed. This thus indicated the strong binding of the NHC ligand **L** at the surface of the NPs, since no free ligand **L** was detected during this experiment and confirm the possible presence of the corresponding protonated ligand **L-H$^+$** in the second coordination sphere of the NPs. A signal at 126.09 ppm was also detected and was tentatively attributed to CO_2 [69].

These NPs were also analysed by solid state NMR: the $^{13}C\{^1H\}$ CP-MAS spectrum of **Rh$^{0.4}$** displayed a series of signals that were assigned as follows: 25.57–29.83 ppm (—CH_3), a single signal at 32.6 ppm (—CH—), an intense signal centred at 127.28 ppm (aromatic carbons), and two more signals with low intensity were detected at *ca.* 140 and 170 ppm (Fig. 5b), that were attributed to **L** and **L-H$^+$**. The fact that these latter signals substantially increased in intensity when a sample of **^{13}C-Rh$^{0.4}$** was analysed by the same technique allowed their unambiguous assignation to the carbenic carbon of both **L** and **L-H$^+$** and reaffirmed the presence of two different species at the NPs surface (Fig. 5d). In the $^{13}C\{^1H\}$ CP-MAS spectrum of **Rh$^{0.4}$** two more broad signals were also detected at 51.48 ppm and 65.88 ppm, which were assigned to the hydrogenated imidazolium backbone (Fig. 5b).

Experiments increasing the time of contact during the acquisition of the $^{13}C\{^1H\}$ CP-MAS NMR spectra (Fig. S34, Supporting information) were also performed to gain further information into the identity of the carbon atoms corresponding to the signals previously detected at *ca.* 140 and *ca.* 170 ppm. The contact time is the delay during which magnetization is transferred from ^1H to ^{13}C and depends on the extent of the dipolar coupling to the proton network that in turn mainly depend on the degree of protonation of each type of carbon. During the experiments performed in this work, the signal centred at *ca.* 170 ppm grew much more slowly, indicating an absence of protons in the close surrounding of this carbon atom. This signal was thus attributed to the C_2-carbon of the ligand coordinated to the Rh surface. Indeed, the detection of spinning side bands in the case of this broad signal detected at *ca.* 170 ppm revealed the static nature of this species. The intensity of the signal at *ca.* 140 ppm grew faster, and was therefore conclusively attributed to **L-H$^+$**.

It was therefore concluded that the NHC-stabiliser was coordinated to the Rh-surface through the C2-position, which corresponds to the less sterically hindered position of the ligand. However, the presence of C4- and C5-coordinated ligands cannot be excluded. Such coordination was previously demonstrated for ILs-stabilised Ir-NPs using deuterium labelling experiments [70].

To study the presence of free sites on the NPs surface by NMR spectroscopy, 0.5 atm of ^{13}CO were added to solid samples of **Rh$^{0.2}$**, **Rh$^{0.4}$** and **Rh$^{0.6}$** at room temperature. In all cases, the appearance of new broad signals between 150 and 200 ppm indicated the coordination of the ^{13}CO on the surface of the NPs (Fig. 5c). The detection of three different signals around 168, 172 and *ca.* 190 ppm is in agreement with the results obtained by IR and the fact that the ^{13}CO could coordinate in geminal (or multicarbonyl) "$Rh(CO)_2$", terminal and bridging mode at the NPs surface. Signals from mobile terminal and geminal ^{13}CO (no apparent spinning sidebands) were detected at 168 and 172 ppm with high intensities due to the proximity to hydrogen carriers from **L** coordinated to edges and apexes of the NPs (Fig. 5c). A signal with lower intensity attributed to bridging ^{13}CO was detected near 190 ppm with spinning sidebands (Fig. S36, Supporting information). The presence of mobile terminal ^{13}COs had previously observed for RuNPs stabilised by PVP [57]. The chemical shifts for coordinated ^{13}CO on the NPs surface are slightly lower than those previously reported for RuNPs (185–250 ppm) [14,15,57,71-73] and closer to values reported for Rh/Silica (177 ppm for terminal and 222 ppm for bridging COs) [74].

2.2. Catalysis

2.2.1. Hydrogenation of phenol derivatives

The hydrogenation of phenol **1** was first carried out using 1.25mol% of **Rh$^{0.2}$** at 30 °C under 20 bar of H_2 in THF and the reaction was monitored by GC–MS. Under these reaction conditions, 95% conversion was reached after 210 min of reaction with selectivities to cyclohexanone (**1a**) and cyclohexanol (**1b**) of 32% and 68%, respectively (Table 1, entry 1).

When the H_2 pressure was decreased to 5 and 1.7 bar, an increase in selectivity to cyclohexanone up to 75% was observed while conversion diminished to 30% for similar reaction time

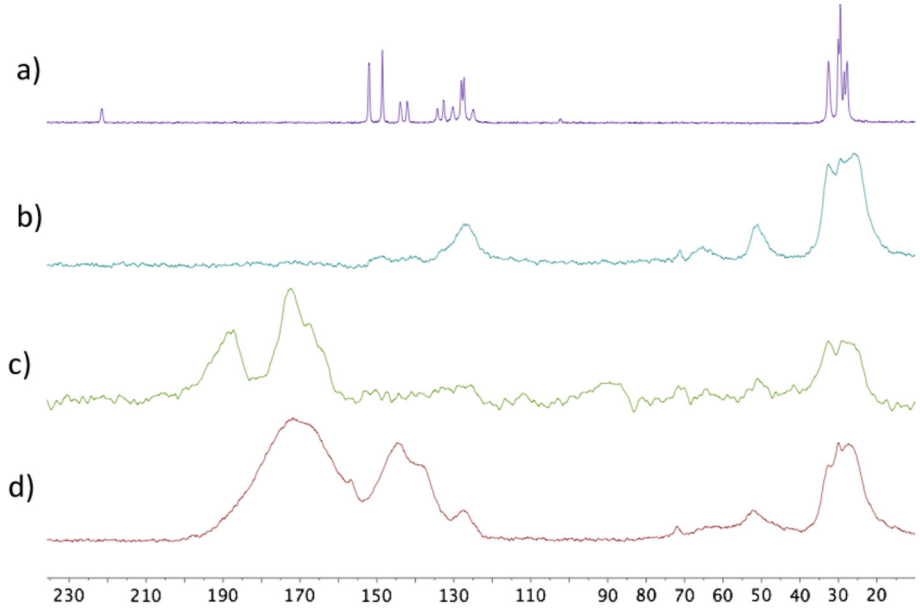

Fig. 5. $^{13}C\{^1H\}$ CP-MAS spectra of (a) L, (b) $Rh^{0.4}$, (c) $Rh^{0.4}$ + CO and (d) ^{13}C-$Rh^{0.4}$.

(Table 1, Entries 2 and 3) [75,76]. However, an increase of temperature up to 60 °C allowed to achieve full conversion with no variation in the selectivity (Table 1, Entry 4). The use of **Rh$^{0.4}$** as catalyst afforded a lower conversion and lower selectivity towards cyclohexanone (**1a**) (Table 1, Entry 5).

The monitoring of the catalytic hydrogenation of **1** using **Rh$^{0.2}$** at 60 °C under 20 and 1.7 bar of H_2 pressure are shown in Scheme 4. When the reduction of **1** was performed under 20 bar of H_2 (Scheme 4a), full conversion was reached after 270 min of reaction. At short reaction times a practically equimolar mixture of **1a** and **1b** was observed, which evolves towards the fully hydrogenated compound **1b**.

When the reaction was conducted at 1.7 bar of H_2, full conversion was achieved at similar reaction times, but in this case, the **1a/1b** ratio (75/25) did not vary over time (Scheme 4b), suggesting that cyclohexanone was not reduced under these conditions. To corroborate this hypothesis, the hydrogenation of cyclohexanone **1a** was carried out using **Rh$^{0.2}$** and **Rh$^{0.4}$** NPs as catalysts. The results showed that **1a** is reduced under 20 bar H_2 but not under 1.7 bar H_2 (see Supporting information). It was therefore concluded that under low H_2 pressure, the selectivity is determined by the difference in rates (k2 *versus* k2′) between isomerisation and hydrogenation of the enol intermediate **1′** (Scheme 5).

Next, the hydrogenation of substituted phenols was explored. When the reaction was performed in the presence of **Rh$^{0.2}$** at 60 °C under 1.7 bar of H_2 pressure, very low conversions were obtained in the hydrogenation of phenol derivatives **2**–**6**. The reactions were then performed at 60 °C and under 20 bar H_2 (Table 2). In all cases, the conversions were lower than when **1** was used as substrate. In agreement with the results obtained in the hydro-

Table 1
RhNPs ($Rh^{0.2}$) catalysed hydrogenation of 1.[a]

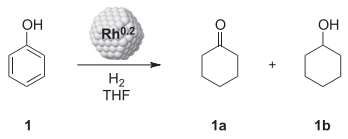

Entry	Pressure (bar)	Temperature (°C)	Conv.[b] (%)	TOF[c] (h^{-1})	**1a**[b] (%)	**1b**[b] (%)
1	20	30	95	81	32	68
2	5	30	93	86	48	52
3	1.7	30	30	23	75	25
4	1.7	60	100	43	79	21
5[d]	1.7	60	62	34	43	57

[a] Conditions: 2.48 mmol substrate, 1.25 mol% **Rh$^{0.2}$**, 20 ml THF, 210 min.
[b] Determined by GC using undecane as internal standard.
[c] TOF = (mmol product/mmol Rh surface) * h^{-1}, calculated at conv.<20%.
[d] 1.25 mol% **Rh$^{0.4}$**.

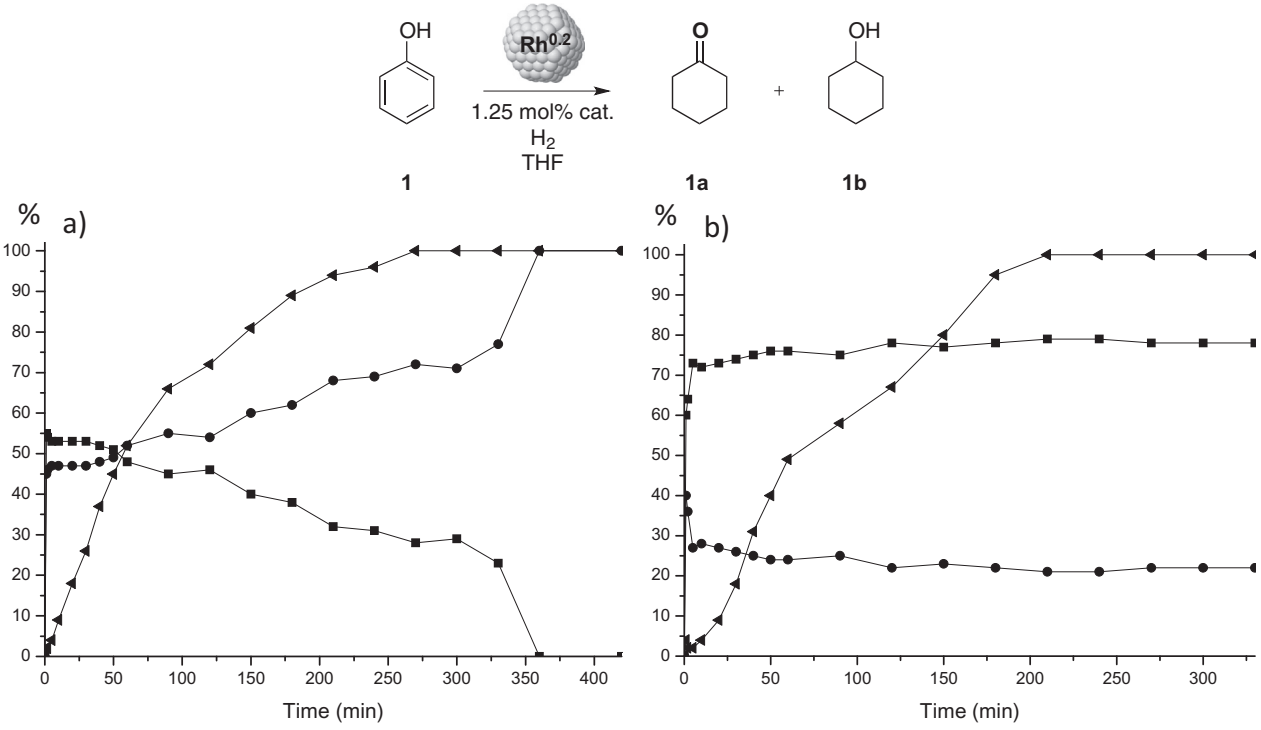

Scheme 4. Monitoring of the catalytic hydrogenation of 1 using $Rh^{0.2}$ as catalyst (a) at 20 bar of H_2, 60 °C (b) 1.7 bar of H_2, 60 °C. (▲) conv.; (■) 1a; (●) 1b.

genation of **1**, the cyclohexanols **2b-6b** were always preferably obtained, although the selectivity to the cyclohexanone **4a** reached 42% (Table 2, Entry 4). The lower selectivities to cyclohexanones obtained with these more sterically hindered substrates are in agreement with the results obtained during the hydrogenation of phenol using **Rh$^{0.4}$** as catalysts (Table 1, Entry 5). Indeed, an increase in steric hindrance either at the surface of the catalyst or at the substrate favours the formation of cyclohexanols, which could indicate that desorption of the enol intermediates is disfavoured, thus enhancing the selectivity to cyclohexanols.

In the case of hydroxyl **5** or alkoxy derivatives **6**, practically no cyclohexanones were detected (Table 2, Entries 5, 6). The cyclohexanol derivatives were obtained as *cis/trans* mixtures with selectivities up to 83:17 (Table 2, Entry 6). These results are in agreement with those previously reported for the hydrogenation of *p*-methylanisole (71:29), *o*-xylene (75:25) and *m*-xylene (75:25) using RhNPs stabilised by P-donor ligand [4], and indicated the desorption of partially reduced species before reaching complete reduction, although restricted (see above) is not fully avoided. It can consequently be concluded that in terms of conversion, substitution of the phenol ring has a detrimental effect, which can be explained by the high steric hindrance provided by the NHC ligand at the catalyst surface.

2.2.2. Reduction of N-heteroaromatic substrates

The hydrogenation of N-heterocyclic compounds using **Rh$^{0.2}$** was evaluated using first pyridine (**7**) as model substrate. Scheme 6 shows the variation of conversion over time at various temperatures and H_2 pressures. As expected, the decrease of both parameters has a negative influence on the conversion, although full conversion could be achieved in 180 min at 30 °C under 10 bar of H_2 pressure.

Rh$^{0.4}$ were applied as catalyst in the hydrogenation of **7** (0.625 mol% cat., 20 bar H_2 at 30 °C) (Fig. S37, Supporting information) and TOF calculated at <20% of conversion was 229 h^{-1}, lower than the calculated for **Rh$^{0.2}$** (305), and in agreement to that observed for previously studied substrates.

With these results in hand, the effect of substituents in *ortho*- and *para*- positions of the pyridine ring was then evaluated. A negative influence of substitution on the conversion was previously reported for 2-methylpyridine [40] and substituted-quinoline derivatives using Rh/Al_2O_3 as catalysts [77]. However, using **Rh$^{0.2}$** as catalyst, the hydrogenation of 2-methylpyridine (**8**) to compound **8a** took place at a similar rate than the parent compound **7** (Scheme 6), whereas the rate of hydrogenation of the 2,6-dimethyl derivative (**9**) to afford **9a** was significantly lower under the same reaction conditions (full conversion was reached extend-

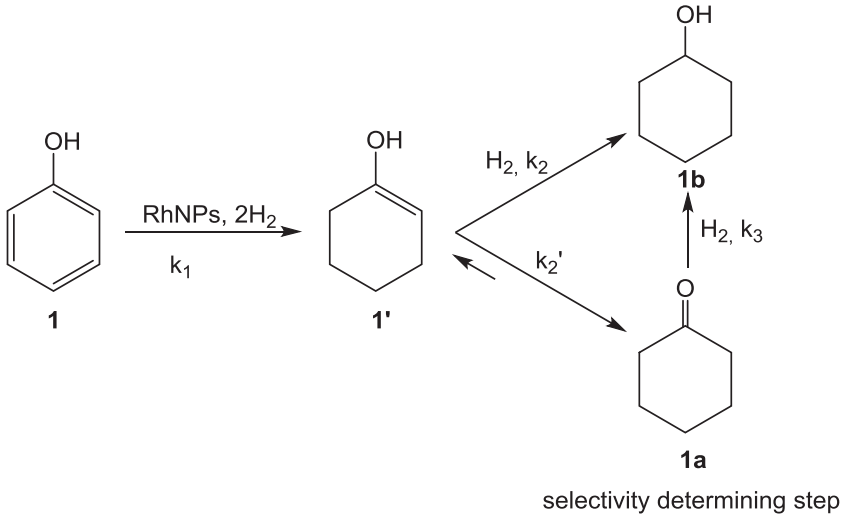

Scheme 5. Competitive reactions in the hydrogenation of phenol using $Rh^{0.2}$ as catalyst.

Table 2
RhNPs ($Rh^{0.2}$) catalysed hydrogenation of phenol derivatives 1–6.[a]

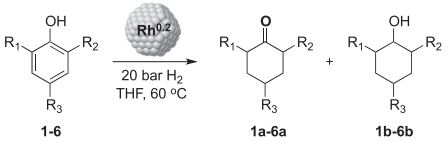

Entry	Substrate	R_1	R_2	R_3	Conv.[b] (%)	**TOF** (h^{-1})[c]	**a**[b] (%)	**b**[b] (%)
1	**1**	—H	—H	—H	96	43	33	67
2	**2**	—CH_3	—H	—H	12	3	27	73 (74:26)[d]
3	**3**	—H	—H	—CH_3	12	3	18	82[e]
4	**4**	—CH_3	—H	—CH_3	8	2	42	58[e]
5	**5**	—OH	—H	—H	38	9	7	93[e]
6	**6**	—OMe	—H	—H	14	3	0	100 (83:17)[d]

[a] Catalytic conditions: 2.48 mmol substrate, 1.25 mol% **Rh$^{0.2}$**, 60 °C, 20 bar H_2, 20 ml THF, 210 min.
[b] Calculated by GC using undecane as internal standard.
[c] TOF = (mmol product/mmol Rh surface) * h^{-1}, calculated at conv.<20%.
[d] *cis:trans* ratio.
[e] Overlapped signals in GC, not quantified.

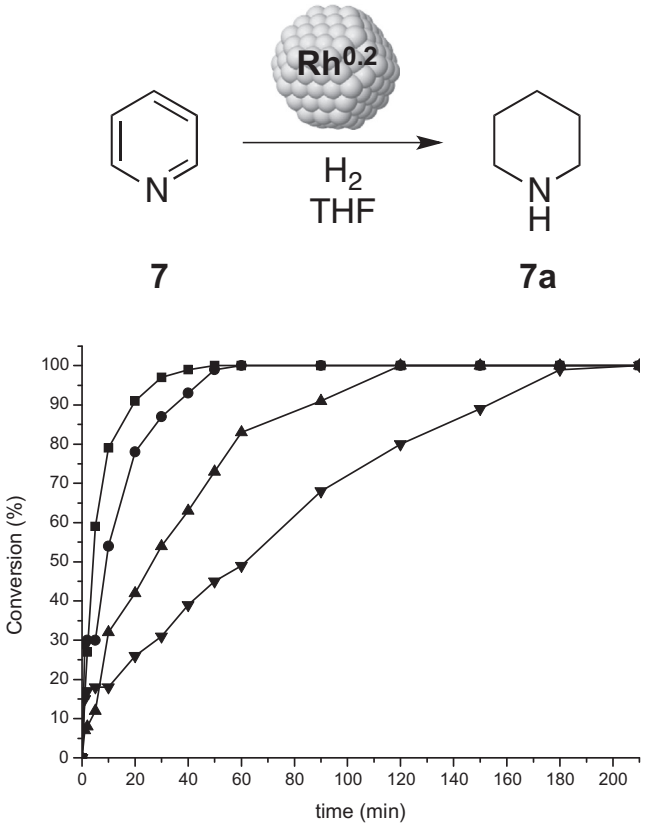

Scheme 6. Monitoring of the catalytic hydrogenation of 7 using $Rh^{0.2}$ as catalyst. (Catalytic conditions: 2.48 mmol substrate, 20 ml THF. (■) 0.625 mol% $Rh^{0.2}$, 60 °C, 20 bar H_2; (●) 1.25 mol% $Rh^{0.2}$, 60 °C, 20 bar H_2; (▲) 0.625 mol% $Rh^{0.2}$, 30 °C, 20 bar H_2; (▼) 0.625 mol% $Rh^{0.2}$, 30 °C, 10 bar H_2).

ing the reaction time) (Fig. 6). In this case, the *cis* diastereoisomer was almost exclusively formed, which suggested a strong interaction between the pyridine ring and the NPs surface, and hence that the decoordination necessary for the formation of the *trans* isomer after partial hydrogenation of the aromatic ring was disfavoured. These results indicated that an increase in the ring substitution negatively influences the hydrogenation rate of these compounds; however, the stereochemistry of the product suggested that the flat coordination of the pyridine ring required for its reduction is strong enough in spite of the presence of two methyl substituents.

In view of these results, the effect of para-substituents was explored using 4-methylpyridine (**10**) and 4-trifluoromethylpyridine (**11**) as substrates. Surprisingly, the hydrogenation of 4-methylpyridine (**10**) to afford **10a** was the slowest of the series (TOF = 38 h^{-1}) (Scheme 5). Hydrogenation of 4-trifluoromethylpyridine (**11**) afforded **11a** at a slightly faster reaction rate (TOF = 48 h^{-1}) than **10**, which indicated that electronically-poorer rings are more easily reduced, in spite of the higher bulkiness of the CF_3 group *vs.* CH_3. These results therefore showed that under these conditions, the hydrogenation rates of para-substituted substrates is more similar to that of 2,6-dimethylderivative **9** than those of **7** and **8**, suggesting that the η^6-coordination of the aromatic ring to the surface of the NPs is more hindered by the presence of substituents in 4-position. This effect was not previously observed when the hydrogenation of 4-methylpyridine was performed using Lewis acid-ILs stabilised RhNPs [40]. In order to confirm this hypothesis, the catalytic hydrogenation of **8** and **10** were carried out using **$Rh^{0.4}$** as catalyst under the same reaction conditions. Lower reaction rates were observed in the reduction of both **8** and **10**, with TOFs of 143 and 19 h^{-1}, respectively (Fig. S38, Supporting information), a bit higher percentage decreases for **10**, which is in agreement with our previous supposition.

In previous studies with Ru and Rh NPs, a different selectivity in ketoarenes reduction (arene *vs.* ketone) was observed depending on the distance between the keto and the arene groups [7,46]. To investigate whether this trend could be extended to pyridine derivatives, the hydrogenation of 2-acetylpyridine (**12**) and 1-pyridin-2-yl-propan-2-one (**13**) was studied.

Hydrogenation of **12** carried out at 30 °C under 20 bar of H_2 afforded full conversion after 60 min of reaction with full selectivity towards the totally reduced product **12d** (Scheme 6a) (TOF = 196 h^{-1}). Full reduction of **12** was previously reported using RuNPs stabilised by PFILs in water (30 °C, 50 bar H_2, 15 h of reaction) [47]. When the H_2 pressure was decreased to 5 bar partially reduced products **12a**, **12b** and **12c** were observed in low selectivities (2, 8 and 14%, respectively) (Scheme 7b), although compound

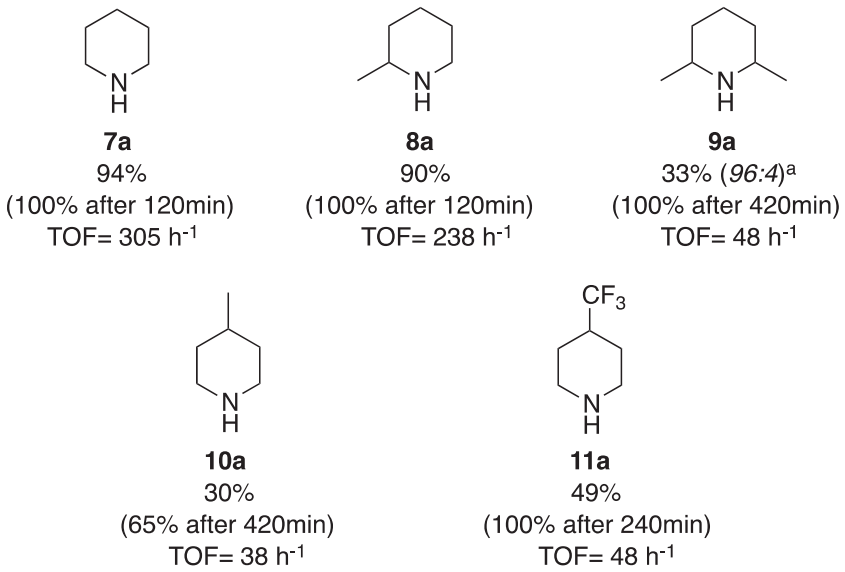

Fig. 6. Hydrogenation of compounds 7–11 to afford 7a-11a using $Rh^{0.2}$ as catalyst. (Conditions: 2.48 mmol substrate, 0.625 mol% $Rh^{0.2}$, 30 °C, 20 bar H_2, 90 min). [a]*cis*/*trans* selectivity.

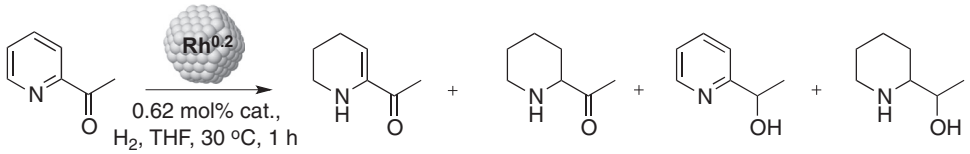

	12	12a	12b	12c	12d
a) 20 bar H_2	100% conv. TOF= 196 h^{-1}	0%	0%	0%	100%
b) 5 bar H_2	84% conv. TOF= 174 h^{-1}	2%	8%	14%	76%

Scheme 7. Hydrogenation of 12 using $Rh^{0.2}$ as catalyst.

12d was again the major product (TOF = 174 h^{-1}). The high activities obtained for the electron-deficient pyridine ring (**12**), compared to **7**, confirmed our assumption that electronically-deficient pyridine rings are more easily reduced.

The reduction of **13** was initially studied at 30 °C and under 5 bar of H_2 (Table 3, Entry 1) in order to explore the possibility to obtain partially reduced compounds. Under these conditions, 79% conversion was obtained after 60 min, which was slightly lower than that obtained for **12** (84%). Interestingly, in this case, the β-enaminone **13a** was the major product of the reaction with 64% selectivity. The identity of this product was confirmed by mass spectrometry (M^+ = 139) (Fig. S90, Supporting information) and ^1H and ^{13}C NMR spectroscopy (Figs. S94 and S95, Supporting information), and comparison with reported values [78]. Products from the selective reduction of the pyridine ring (**13b**), ketone (**13c**) and the totally reduced product (**13d**) were also detected in 8, 16 and 12%, respectively. At longer reaction time, the reduction of **13b** and **13c** into **13d** was observed whereas the selectivity to **13a** remained unchanged even after 4 h of reaction under these conditions (Table 3, Entry 2). When the reaction was repeated under 2 bar of H_2 pressure, an increase in the selectivity to **13a** up to 78% was observed (Table 3, Entry 3). This selectivity was maintained when the reaction was run for 240 min (conv. = 89%) (Table 3, Entry 4).

For comparison purposes, the reduction of arylketones **14**–**16** was explored using the same catalyst $\mathbf{Rh^{0.2}}$.

The hydrogenation of **14** in the presence of $\mathbf{Rh^{0.2}}$ at 30 °C and under 20 bar H_2 revealed much slower than that of **12** under the same conditions, and 5h of reaction were necessary to achieve full conversion. The product corresponding to the selective reduction of the keto group was not detected and a ratio **14a/14c** = 45:55 was obtained at full conversion (Table 4, Entry 1). In view of this result, the catalyst $\mathbf{Rh^{0.4}}$ was tested to check whether higher ligand coverage could have an influence on the selectivity, but similar results were obtained although the reaction was a bit slower (Table 4, Entry 2). Reduction of **15** under the same conditions furnished the same results for both catalysts but, in this case, no fully reduced product **14c** was detected and an equimolar mixture of **15a** and **15 b** was obtained (Table 4, Entries 1 and 2 *vs.* 3 and 4). The lack of reduction of **15b** using RhNPs stabilised by phosphine ligands under similar reaction conditions was previously reported by our group [7].

However, a significant change in selectivity in favour of the reduction of the aromatic ring was observed when **16** was used as substrate, achieving values of 91% for the formation of 4-cyclohexylbutan-2-one (**16a**) using both $\mathbf{Rh^{0.2}}$ and $\mathbf{Rh^{0.4}}$ nanocatalysts (Table 4, Entries 5 and 6).

The monitoring of the reaction in the presence of $\mathbf{Rh^{0.2}}$ revealed lower reaction rates than in the hydrogenation of **14**, achieving full conversion of the starting material after 110 min of reaction with a TOF of 147 h^{-1} (Fig. S41, Supporting information).

The trend observed in the reduction of the arylketones **14**–**16** in the presence of the nanocatalysts $\mathbf{Rh^{0.2}}$ and $\mathbf{Rh^{0.4}}$ is in agreement to that previously reported with Ru/NHC and Rh/PPh_3 systems [7,46].

Comparison of the results obtained in the hydrogenation of the pyridine derivative **13** and the related arylketone **15** indicated a clearly distinct output. The product **13a** is probably formed through isomerization of a partially reduced intermediate, which takes place faster on this case than for **15** (Scheme 8).

Next, the competitive reduction of pyridine *vs.* phenyl rings was looked at. With this purpose we studied first the hydrogenation of

Table 3
RhNPs ($Rh^{0.2}$) catalysed hydrogenation of 13.[a]

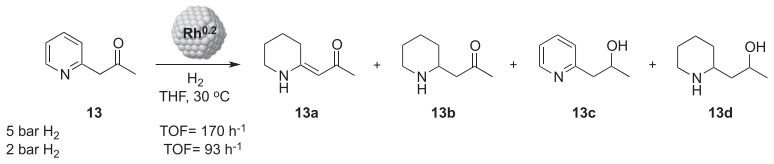

Entry	Time (min.)	Pressure (bar)	Conv.[b] (%)	**13a**[b] (%)	**13b**[b] (%)	**13c**[b] (%)	**13d**[b] (%)
1	60	5	79(100)[c]	64	8	16	12
2	240	5	100	64	0	0	36
3	60	2	39	78	12	10	0
4	240	2	89	76	12	9	3

[a] Catalytic conditions: 2.48 mmol substrate, 0.625 mol% $\mathbf{Rh^{0.2}}$.
[b] Calculated by GC using undecane as internal standard.
[c] After 120 min of reaction.

Table 4
RhNPs ($Rh^{0.2}$, $Rh^{0.4}$) catalysed hydrogenation of aromatic ketones (14, 15, 16).[a]

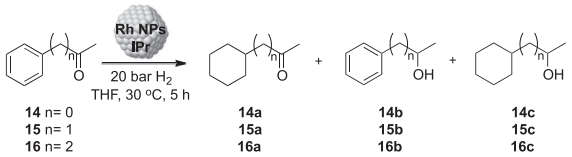

Entry	Substrate	Catalyst	Conversion[b] (%)	**TOF** (h^{-1})	**a**[b] (%)	**b**[b] (%)	**c**[b] (%)
1	**14**	**$Rh^{0.2}$**	100	457	45	–	55
2	**14**	**$Rh^{0.4}$**	100	99	55	3	42
3	**15**	**$Rh^{0.2}$**	100	–[c]	50	50	–
4	**15**	**$Rh^{0.4}$**	100	–[c]	53	47	–
5	**16**	**$Rh^{0.2}$**	100	147	91	7	2
6	**16**	**$Rh^{0.4}$**	100	–[c]	91	7	2

[a] Catalytic conditions: 2.48 mmol substrate, 1.25 mol% cat.
[b] Calculated by GC using undecane as internal standard.
[c] TOF has not been measured.

benzene (**17**) under the same reaction conditions than those used for pyridine (**7**) (Scheme 9). After 60 min, 84% conversion was obtained, similarly to the results obtained for **7**. However, when the hydrogenation of a 1:1 mixture of **7**:**17** was carried out and monitored by GC over time, complete conversion of **7** was reached when hydrogenation of **17** was only 9% of conversion (Scheme 10).

These results can be explained considering that piperidine (**7a**), which is produced by the reduction of **7**, can coordinate to the NPs surface and as such can act as a poison that prevent the reduction of **17**. This poisoning effect has been previously evidenced in the reduction of quinoline and imines using nanocatalysts [79]. The fact that pyridine **7** was reduced in the presence of piperidine **7a** suggests a displacement of the reduction product **7a** by the substrate **7**, which confirms the involvement of the nitrogen coordination with the catalyst surface prior to hydrogenation.

Next, the hydrogenation of 2-phenylpyiridine (**18**) was looked at 30 °C under 20 bar of H_2 and the reaction was monitored over time (Scheme 11a). Under these conditions, this reaction was very slow (19% conv. after 7 h). The low reactivity of 2-phenylpyridines had been already observed [80]. Three products **18a-c** can be formed and initially only **18a,b** were produced in a ratio 65:35. Compound **18b** was slowly reduced to **18c**, but **18a** was not reduced under these conditions, and a constant ratio **18a/(18b +18c)** was observed over time, corresponding to the selectivity for the pyridine *vs.* arene reduction.

When the temperature was increased to 60 °C, an increase in activity was observed (Scheme 11b) and compound **18c** was rapidly generated. Under these conditions, the compound **18a** was also reduced and, after 48 h, only the fully reduced product (**18c**) was present in the reaction mixture.

To summarize, both the pyridine moiety and the phenyl ring were reduced using **$Rh^{0.2}$** as catalyst at 20 bar of H_2 and 60 °C to afford the fully reduced product **18c** in 100% selectivity.

Next, the hydrogenation of quinoline **19** was investigated and was initially performed at 30 °C under 20 bar of H_2 using **$Rh^{0.2}$** as catalysts, and the reaction monitored by GC (Scheme 12a). Under these conditions, full conversion was achieved after 140 min of reaction. Initially, the fully reduced product **19c** was not detected and the ratio **19a/19b** was 89:11 (conversion 33%, Scheme 12a). This selectivity progressively decreased to 75:20 when full conversion was achieved. At this point, 5% of **19c** was

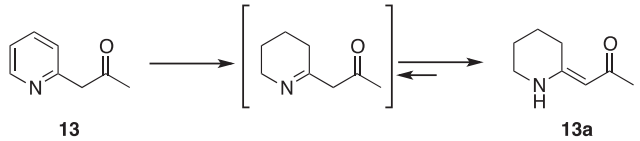

Scheme 8. Proposed isomerization mechanism for the formation of 13a.

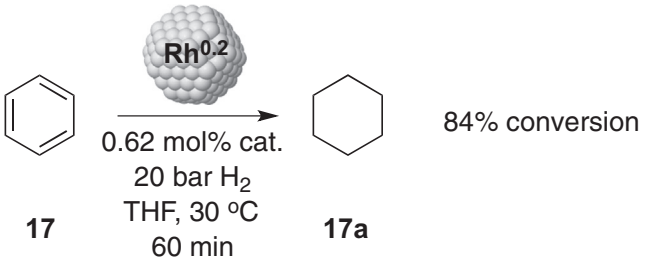

Scheme 9. Hydrogenation of 17 using $Rh^{0.2}$ as catalyst.

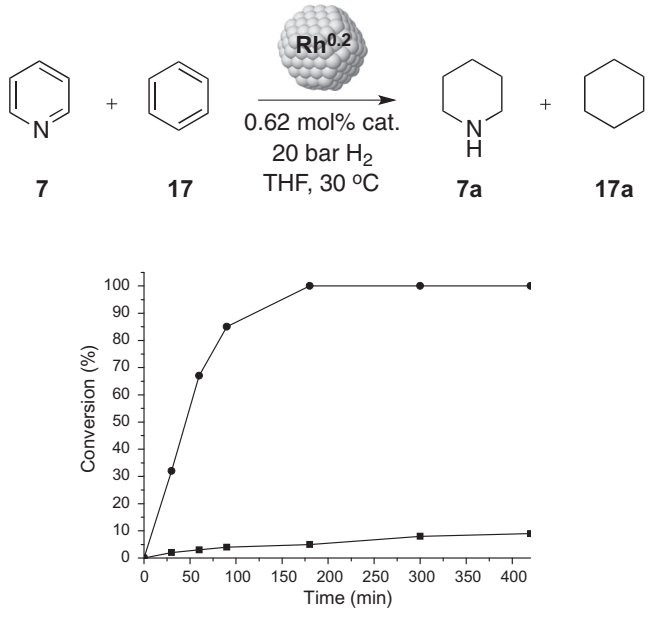

Scheme 10. Monitoring of the catalytic hydrogenation of 7 + 17 using $Rh^{0.2}$ as catalyst. (●) 7; (■) 17.

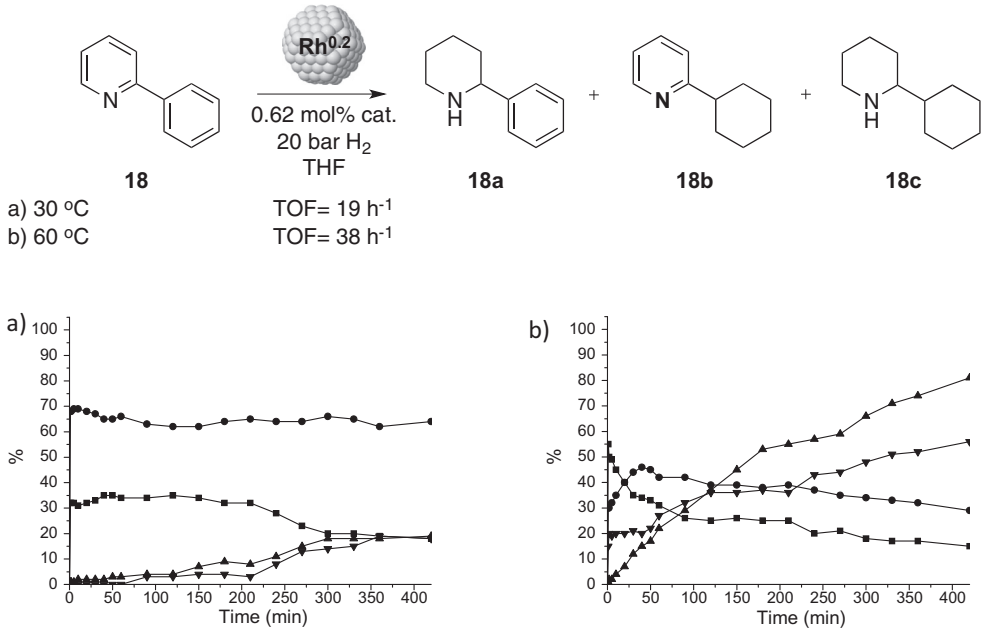

Scheme 11. Monitoring of the catalytic hydrogenation of 18 using $Rh^{0.2}$ at (a) 30 °C and (b) 60 °C. (▲) conv.; (●) 18a; (■) 18b; (▼) 18c.

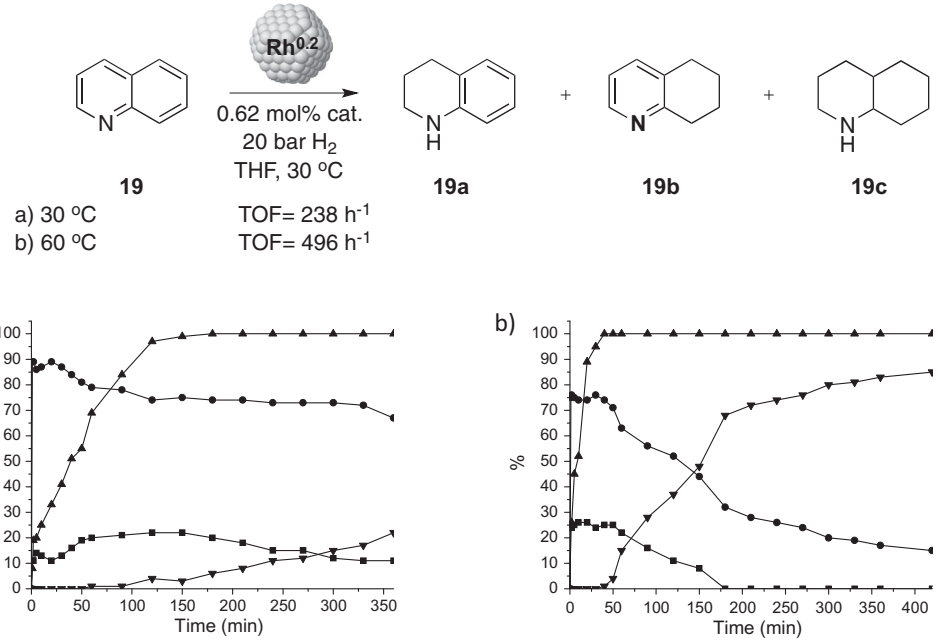

Scheme 12. Monitoring of the catalytic hydrogenation of 19 using (a) $Rh^{0.2}$ at 30 °C and (b) $Rh^{0.2}$ at 60 °C (▲) conv.; (●) 19a; (■) 19b; (▼) 19c.

formed although the reduction of both **19a** and **19b** was very slow under these conditions.

When the reaction was conducted at 60 °C, full conversion was achieved after only 30 min of reaction and at this point ratio **19a/19b** was 75:25 (TOF = 496 h^{-1}) (Scheme 12b), with practically no traces of the fully reduced product **19c**. After 24 h of reaction, full conversion towards **19c** was achieved as a consequence of the complete reduction of **19a,b**. In summary, in the presence of $\mathbf{Rh^{0.2}}$ as catalyst, **19c** can be obtained as the only product after 24 h in the absence of additives [37,52,53]. The TOF measured for this last process (496 h^{-1}) is the highest reported to date.

When $\mathbf{Rh^{0.4}}$ was used as catalyst for the hydrogenation of **19** under the same conditions, selectivities were similar to those obtained with $\mathbf{Rh^{0.2}}$, although a slight decrease in the reaction rate was observed (TOF = 447 h^{-1}) (Fig. S42, Supporting information). These results confirmed the lower activity of the catalyst with a higher coverage of stabilising ligand at its surface.

In conclusion, here we report the synthesis of small and well-defined Rh nanoparticles stabilised by 0.2, 0.4 and 0.6 equivalent of the NHC ligand **L** and their full characterization using several techniques. In all cases, the co-existence of two different stabilising species coordinated to the NPs surface, namely the NHC carbene ligand **L** and its protonated counterpart $\mathbf{L\text{-}H^{+}}$, was observed by solution and solid state NMR. It is noteworthy that the NPs obtained using 0.4 and 0.6 equivalent of **L** displayed very similar features, which indicates the saturation of the surface using [**L**]/

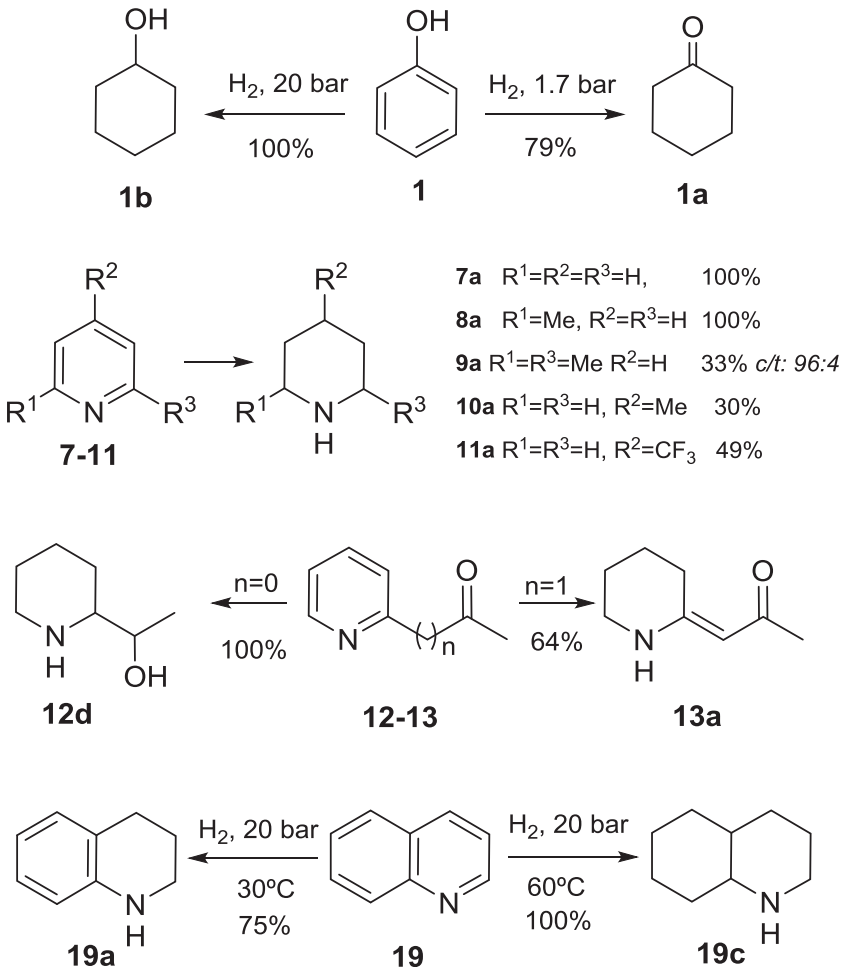

Scheme 13. Summary of catalytic results using $Rh^{0.2}$.

[Rh] molar ratio >0.4. Exposition to CO in correlation with spectroscopic techniques provided evidence for the availability of 3 types of sites at the surface of these nanoparticles and indicated the location of the ligands on the faces, edges and apexes of the NPs. These studies showed that the use of an excess of ligand during their synthesis induce their coordination on the faces of the RhNPs. Under high CO pressures, the strong binding of the carbene to the Rh surface was confirmed since no free **L** could be detected while the formation of a Rh(I)-NHC complex was observed in solution. Interestingly, **L-H$^+$** was not displaced from the NPs surface by reaction with PPh_3 and $P(OPh)_3$ but was removed from the surface under 30 bar of CO.

$Rh^{0.2}$ NPs resulted to be active catalyst in the reduction of phenol, pyridine and derivatives and quinoline (Scheme 13). In the reduction of phenol, selectivities up to 79% to the formation of cyclohexanone (**1a**) or 100% towards cyclohexanol (**1b**) can be obtained depending on the reaction conditions. This catalytic system exhibited much lower activity in the hydrogenation of substituted phenols. Pyridine was easily hydrogenated, faster than benzene, and reaction of 2- and 2,6-substituted pyridines was slower but full conversion could be achieved. Interestingly, the hydrogenation of 4-methyl and 4-trifluoromethylpyridine resulted particularly slow (slower than that of 2-methylpyridine), which indicate a high sensitivity of this catalyst to the size of the substrate. 2-acetylpyridine (**12**) was fully reduced in a short reaction time (faster than pyridine), while the hydrogenation of 1-(pyridin-2-yl)propan-2-one (**13**) provided β-enaminone **13a** (selectivity 64% at full conversion, but achieves 76% at 89% of conversion) as a consequence of the partial reduction of the pyridine ring followed by isomerization. Hydrogenation of arylketones followed the previously reported trend, and high selectivity towards selective arene hydrogenation was achieved when the substrate contains at least two methylene groups between the arene and keto groups. Quinoline (**19**) could be either partially hydrogenated to 1,2,3,4-tetrahydroquinoline (**19a**) with a 75% of selectivity at full conversion, or fully reduced to **19c** by adjusting the reaction conditions.

3. Experimental section

3.1. General procedures

All operations were carried out using standard Schlenk tubes, Fischer-Porter bottle techniques or in a glove-box under argon atmosphere. The chemicals were purchased from Sigma-Aldrich and used without further purification. THF and pentane were dried over sodium/benzophenone, distilled and then thoroughly degassed before use by three freeze- pump cycles. IPr carbene [81,82] and [Rh(η^3-C_3H_5)$_3$] [83,84] were synthesized from previously published methodologies.

^{1}H and ^{13}C, spectra were recorded on a Varian® Mercury VX 400 (400 MHz and 100.6 MHz respectively). Chemical shift values for ^{1}H and ^{13}C were referred to internal $SiMe_4$ (0.0 ppm). Chemical shifts are reported in parts per million (ppm) and coupling constants are reported in Hertz (Hz). Mass spectra was recorded on

a Finnigan MAT 900S (EB-Trap Geometry) Syringes pump Model 22.

Solid state $^{13}C\{^1H\}$-Cross Polarization- magic Angle Spinning (CPMAS) experiments were performed on a BRUKER Avance III spectrometer operating at a magnetic field of 9.4 T and equipped with a double channel 4.0 mm MAS probe. The powder materials were packed into 4 mm ZrO_2 rotors and were sealed with tight fitting Kel-F caps. Sample spinning was set to 12 kHz in all experiments. Chemical shifts are reported in parts per million (ppm) externally referenced to adamantane (CH_2 peak set to 38.5 ppm). Cross polarization time was set to 2500 ms and performed with a radio-field strength of 83 kHz and a ^1H ramp pulse was used (ramp70100 in Bruker nomenclature). ^1H-decoupling was performed using SPINAL-64 pulse scheme. The recovery delay was set to 1 s and overall experimental time was set from 12 to 24 h by varying the number of scans depending on the sample sensitivity. Spectra were acquired at 20°C controlled by a BRUKER BCU unit.

Transmission Electron Microscopy (TEM) analysis were performed at the "Unitat de Microscopia dels Serveis Cientificotècnics de la Universitat Rovira i Virgili" (TEM-SCAN) in Tarragona with a Zeiss 10 CA electron microscope operating at 100 kV with resolution of 3 Å. The particles size distributions were determined by a manual analysis of enlarged images. At least 300 particles on a given grid were measured in order to obtain a statistical size distribution and a mean diameter. For High Resolution Transmission Electron Microscopy (HRTEM) and Scanning Electron Microscopy (SEM) a probe-corrected, cold-FEG JEOL ARM microscope equipped with a centurio EDX detector operated at 200 keV was used.

X-ray diffraction (XRD) measurements were made using a Siemens D5000 difractometer (Bragg Brentano parafocusing geometry and vertical θ–θ goniometer) fitted with a curved graphite diffracted beam monochromator, incident and diffracted beam Soller slits, a 0.06° receiving slit and scintillation counter as a detector. The angular 2θ diffraction range was between 26 and 95°. The data were collected with an angular step of 0.05° at 16s per step and sample rotation. A low background Si(5 1 0) wafer was used as Sample holder. $Cu_{k\alpha}$ radiation was obtained from a copper X-ray tube operated at 40 kV and 30 mA.

Wide-angle X-ray scattering (WAXS) was performed at CEMES-CNRS. Samples were sealed in 1 mm diameter Lindemann glass capillaries. The samples were irradiated with graphite-monochromatized molybdenum Kα (0.071069) radiation and the X-ray intensity scattered measurements were performed using a dedicated two-axis diffractometer. Radial distribution functions (RDF) were obtained after Fourier Transformation of the reduced intensity functions.

X-ray photoelectron spectroscopy (XPS) analysis were performed at the "Centres Científics i Tecnològics de la Universitat de Barcelona" (CCiT UB) in a PHI 5500 Multitechnique System (from Physical Electronics) with a monochromatic X-Raysource (Aluminium Kalfa line of 1486.6 eV energy and 350 W), placed perpendicular to the Analyser axis and calibrated using the 3d5/2 line of Ag with a full width at half maximum (FWHM) of 0.8 eV. The analysed area was a circle of 0.8 mm diameter, and the selected resolution for the spectra was 187.5 eV of Pass Energy and 0.8 eV/step fort the general spectra and 23.5 eV of Pass Energy and 0.1 eV/step for the spectra of the different elements in the depth profile spectra. A low energy electron gun (<10 eV) was used in order to discharge the surface when necessary. All measurements were performed in an ultra high vacuum (UHV) chamber pressure between 5×1039 and 2×1038 torr. For this analysis, the data processing was carried out with the program CasaXPS. Initially, the general spectrum of the different binding energies observed for this sample was analysed and was used to calibrate the following calculations. This calibration was performed using the values for the rhodium that is the element of interest for these analyses.

Thermogravimetric (TGA) analysis was carried out in the furnace of a Mettler Toledo TGA/SDTA851 instrument. As a typical TGA experiment, 132 mg of NPs were placed in the simple holder in the furnace and the material was heated up at a rate of 10 °C/min in N_2, while the weight was recorded continuously from 30 °C to 900 °C. The weight loss of the organic part and the metal were used to calculate an approximate number of ligands coordinated to the metal surface. The ligand loss was attributed to the weight loss observed between 150 and 900 °C. For the calculation, the molecular weight of the corresponding ligands and the metal, and the number of metal atoms at the surface from TEM data were taken into account.

Infrared spectroscopy (IR) analysis was performed by the preparation of samples as KBr pellets. The nanoparticles were used without any preparation step, mixed and crushed with dry KBr in the glove box before the preparation of the pellet. For CO coordination studies, Rh nanoparticles were introduced in a Fischer Porter bottle and were pressurised with 3 bar of H_2 in solid state for 5 h. After this period of time, the H_2 gas was evacuated under vacuum for 10 min. The Fischer Porter bottle was then pressurised with 1 atm of CO for 16 h. Then, the gas was evacuated under vacuum for 15 min and IR spectroscopy samples were prepared as KBr pellets in the glove box.

3.2. General procedure for the synthesis of Rh NPs stabilised by IPr

In a typical procedure, the $[Rh(\eta^3\text{-}(C_3H_5)_3]$ (250 mg, 0.22 mmol) was placed into a Fischer-Porter reactor and dissolved in 230 ml of dry and deoxygenated THF by three freeze-pump cycles. The resulting yellow solution was cooled at -110 °C (acetone/N_2 bath) and a solution of 20 ml of THF containing the appropriate amount of equivalents of the IPr carbene was added into the reactor. The Fischer-Porter reactor was then pressurized under 4 bar H_2 and stirred for 30 min at room temperature. The solution was then heated to 35 °C and stirred at this temperature during 16 h. The initial yellow solution became black after 1 h. A small amount (2 drops approx.) of the solution was deposited under an Argon atmosphere on a carbon-covered copper grid for transmission electron microscopy analysis. The rest of the solution was evaporated to dryness. Precipitation and washings with pentane (3×15 ml) was then carried out, obtaining a black powder. (Yield: ca. 150 mg, 98%). A similar procedure was followed for the synthesis of the ^{13}C-Rh NPs in similar yields.

3.3. General procedure for the catalytic hydrogenation reactions

Autoclave Par 477 equipped with PID control temperature and reservoir for kinetic measurements and HEL 24 Cat reactor for substrate scope were used as reactors for the hydrogenation reactions. In a typical experiment, the autoclave was charged in the glovebox with the desired Rh NPs (1.25 or 0.625 mol%; the catalyst concentration was calculated based on the total number of metallic Rh atoms in the surface of the NPs) and the substrate (0.124 M) in THF. Molecular hydrogen was then introduced until the desired pressure was reached and the reaction was stirred for the desired reaction time at the selected temperature. At the end of the reaction, the autoclave was depressurised and the solution was filtered through silica for subsequent analysis by GC. The conversion and selectivities for each reaction product were determined by GC-FID on an Agilent Technologies 7890A spectrometer, with a HP-5 column ($30m \times 0.25$ mm $\times 0.25$ μm) using undecane as internal standard. TOF was defined as moles of products per mol Rh at the surface of the NPs per hour.

Acknowledgements

The authors would like to acknowledge financial support from the Universitat Rovira i Virgili – Spain (Grant Marti Franquès 2013PMF-PIPF-90), the Spanish Ministerio de Economía y Competividad and the Fondo Europeo de Desarrollo Regional FEDER (CTQ2016-75016-R, AEI/FEDER, UE), and the Generalitat de Catalunya – Spain (2014SGR670).

Appendix A. Supplementary material

Supplementary data associated with this article can be found, in the online version, at http://dx.doi.org/10.1016/j.jcat.2017.08.010.

References

[1] (a) G.A. Somorjai, H. Frei, J.Y. Park, J. Am. Chem. Soc. 131 (2009) 16589–16605; (b) K. Philippot, in: R.H. Crabtree, M.P. Mingos, D. O'Hare (Eds.), B. Chaudret in Comprehensive Organometallic Chemistry III, Elsevier, Amsterdam, 2007, p. 71.
[2] D. Astruc (Ed.), Nanoparticles and Catalysis, Wiley-VCH, Weinheim, 2007.
[3] (a) J.A. Widegren, R.G. Finke, J. Mol. Catal. A: Chem. 191 (2003) 187–207; (b) A. Roucoux, Top. Organomet. Chem. 16 (2005) 261–279; (c) A. Roucoux, J. Schultz, H. Patin, Chem. Rev. 102 (2002) 3757–3778; (d) A. Stanislaus, B.H. Cooper, Catal. Rev. Sci. Eng. 36 (1994) 75.
[4] J. Ll, A. Castelbou, E. Gual, C. Mercadé, C. Godard Claver, Catal, Sci. Technol. 3 (2013) 2828–2833.
[5] A. Gual, C. Godard, K. Philippot, B. Chaudret, A. Denicourt-Nowicki, A. Roucoux, S. Castillón, C. Claver, ChemSusChem 2 (2009) 769–779.
[6] D. González-Gálvez, P. Nolis, K. Philippot, B. Chaudret, P.W.N.M. van Leeuwen, ACS Catal. 2 (2012) 317–321.
[7] J. Ll, E. Castelbou, P. Bresó-Femenia, B. Blondeau, S. Chudret, C. Claver Castillón, C. Godard, ChemCatChem 6 (2014) 3160–3168.
[8] E. Bresó-Femenia, B. Chaudret, S. Castillón, Catal, Sci. Technol. 5 (2015) 2741–2751.
[9] I. Cano, M.J.-L. Tschan, L.M. Martínez-Prieto, K. Philippot, B. Chaudret, P.W.N.M. van Leeuwen, Catal, Sci. Technol. 6 (2016) 3758–3766.
[10] I. Cano, A.M. Chapman, A. Urakawa, P.W.N.M. van Leeuwen, J. Am. Chem. Soc. 136 (2014) 2520–2528.
[11] (a) P. Liu, R. Qin, Q. Fu, N. Zheng, J. Am. Chem. Soc. 139 (2017) 2122; (b) P. Serp, K. Philippot (Eds.), Nanomaterials in Catalysis, Wiley-VCH Verlag GmbH & Co. KGaA, Weinheim, 2013; (c) L. Starkey Ott, R. Finke, G, Coord. Chem. Rev. 251 (2007) 1075–1100, for a critical review concerning the role of different types of capping agents in the stabilization of metal nanoparticles.
[12] P. Lara, K. Philippot, B. Chaudret, ChemCatChem 5 (2013) 28–45.
[13] P. Lara, O. Rivada-Wheelaghan, S. Conejero, R. Poteau, K. Philippot, B. Chaudret, Angew. Chem. Int. Ed. 50 (2011) 12080–12084.
[14] P. Lara, L.M. Martínez-Prieto, M. Roselló-Merino, C. Richter, F. Glorius, S. Conejero, K. Philippot, B. Chaudret, Nano-Struct. & Nano-Objects 6 (2016) 39–45.
[15] L.M. Martínez-Prieto, A. Ferry, P. Lara, C. Richter, K. Philippot, F. Glorius, B. Chaudret, Chem. Eur. J. 21 (2015) 17495–17502.
[16] L.M. Martínez-Prieto, A. Ferry, L. Rakers, C. Richter, P. Lecante, K. Philippot, B. Chaudret, F. Glorius, Chem. Commun. 52 (2016) 4768–4771.
[17] C. Richter, K. schaepe, F. Glorius, B.J. Ravoo, Chem. Commun. 50 (2014) 3204–3207.
[18] J.M. Asensio, S. Tricard, Y. Coppel, R. Andrés, B. Chaudret, E. de Jesús, Angew. Chem. Int. Ed. 56 (2017) 865–869.
[19] P. Lara, A. Suárez, V. Collière, K. Philippot, B. Chaudret, ChemCatChem 6 (2014) 87–90.
[20] E.A. Baquero, S. Tricard, J.C. Flores, E. de Jesús, B. Chaudret, Angew. Chem. Int. Ed. 53 (2014) 13220–13224.
[21] C.J. Serpell, J. Cookson, A.L. Thompson, C.M. Brown, P.D. Beer, Dalton Trans. 42 (2013) 1385–1393.
[22] E.C. Hurst, K. Wilson, I.J.S. Fairlamb, V. Chechik, New. J. Chem. 33 (2009) 1837–1840.
[23] J. Vignolle, T.D. Tilley, Chem. Commun. (2009) 7230–7232.
[24] X. Ling, N. Schaeffer, S. Roland, M.-P. Pileni, Langmuir 29 (2013) 12647–12656.
[25] C. Zhao, J. He, A.A. Lemonidou, X. Li, J.A. Lechter, J. Catal. 280 (2011) 8–16.
[26] N. Yan, Y. Yuan, R. Dykeman, Y. Kou, P.J. Dyson, Angew. Chem. Int. Ed. 49 (2010) 5549–5553.
[27] K.L. Luska, P. Migowski, S. El Sayed, W. Leitner, Angew. Chem. Int. Ed. 54 (2015) 15750–15755.
[28] L. Chen, J. Xin, L. Ni, H. Dong, D. Yan, X. Lu, S. Zhang, Green Chem. 18 (2016) 2341–2352.
[29] X. Cui, A.-E. Surkus, K. Junge, C. Topf, J. Radnik, C. Kreyenschulte, M. Beller, Nat. Commun. 7 (2016) 11326.
[30] U. Schuchardt, D. Cardoso, R. Sercheli, R. Pereira, R.S. da Cruz, M.C. Guerreiro, D. Mandellif, E.V. Spinacé, E.L. Pires, Appl. Catal. A. 211 (2001) 1–17.
[31] World Nylon 6 & 66 Supply/Demand Report, PCI-Fibers & Raw Materials, Seaford, UK, 1998.
[32] a) N. Yan, Y. Yuan, P.J. Dyson, Chem. Commun. 47 (2011) 2529–2531; b) J. Zhang, M. Ibrahim, V. Collière, H. Asakura, T. Tanaka, K. Teramura, K. Philippot, N. Yan, J. Mol. Catal. A.: Chem 422 (2016) 188–197; c) A. Roucoux, J. Schulz, H. Patin, Adv. Synth. Catal. 345 (2003) 222–229.
[33] I.E. Ertas, M. Gulcan, A. Bulut, M. Yurderi, J. Mol. Catal. A.: Chem. 410 (2015) 209–220.
[34] A.L. Maksimov, S.N. Kuklin, Y.S. Kardasheva, E.A. Karakhanov, Pet. J. 53 (2013) 177–184.
[35] V. Mévellec, A. Roucoux, E. Ramirez, K. Philippot, B. Chaudret, Adv. Synth. Catal. 346 (2004) 72–76.
[36] a) Y. Wang, J. Yao, H. Li, D. Su, M. Antonietti, J. Am. Chem. Soc. 133 (2011) 2362–2365; b) G. Feng, P. Chen, H. Lou, Catal, Sci. Technol. 5 (2015) 2300–2304; c) F. Zhang, S. Chen, H. Li, X.-M. Zhang, H. Yang, RSC Adv. 5 (2015) 102811–102817; d) A. Chen, G. Zhao, J. Chen, L. Chen, Y. Yu, RSC Adv. 3 (2013) 4171–4175; e) J.-F. Zhu, G.-H. Tao, H.-Y. Liu, L. He, Q.-H. Sun, H.-C. Liu, Green Chem. 16 (2014) 2664–2669; f) Z. Li, J. Liu, C. Xia, F. Li, ACS Catal. 3 (2013) 2440–2448; g) C.-J. Lin, S.-H. Huang, N.-C. Lai, C.-M. Yang, ACS Catal. 5 (2015) 4121–4129.
[37] M. Fang, N. Machalaba, R. Sánchez-Delgado, Dalton Trans. 40 (2011) 10621–10632.
[38] Y. Motoyama, M. Takasaki, S.-H. Yoon, I. Mochida, H. Nagashima, Org. Lett. 21 (2009) 5042–5045.
[39] A. Sánchez, M. Fang, A. Ahmed, R.A. Sánchez-Delgado, Appl. Catal. A 477 (2014) 117–124.
[40] A. Karakulina, A. Gopakumar, I. Akçok, B.L. Roulier, T. LaGrange, S.A. Katsyuba, S. Das, P.J. Dyson, Angew. Chem. Int. Ed. 55 (2016) 292–296.
[41] Y. Zhang, G.-Y. Fan, L. Wang, R.-X. Li, H. Chen, X.-J. Li, Acta. Phys. –Chim. Sin. 25 (2009) 2270–2274.
[42] M.L. Buil, M.A. Esteruelas, S. Niembro, M. Olivá, L. Orzechowski, C. Pelayo, A. Vallribera, Organometallics 29 (2010) 4375–4383.
[43] V. Mévellec, A. Roucoux, Inorg. Chim. Acta 357 (2004) 3099–3103.
[44] T. Harada, S. Ikeda, Y.H. Ng, T. Sakata, H. Mori, T. Torimoto, M. Matsumura, Adv. Funct. Mater. 18 (2008) 2190–2196.
[45] R.A. Murphy, A.Y. Chen, S.K. Nair, G.M. Gallego, N.W. Sach, G. Smith, Tetrahedron Lett. (2016) 5588–5591.
[46] D. Gonzalez-Galvez, P. Lara, O. Rivada-Wheelaghan, S. Conejero, B. Chaudret, K. Philippot, P.W.N.M. van Leeuwen, Catal, Sci. Technol. 3 (2013) 99–105.
[47] H.-Y. Jiang, X.-X. Zheng, Catal, Sci. Technol. 5 (2015) 3728–3734.
[48] M. Fang, R.A. Sánchez-Delgado, J. Catal 311 (2014) 357–368.
[49] G. Perot, Catal. Today 10 (1991) 447.
[50] (a) R.T. Shuman, P.L. Omstein, J.W. Paschal, P.D. Gesellchem, J. Org. Chem. 55 (1990) 738; (b) J.M. Schaus, D.L. Huser, R.D. Titus, Synth. Commun. 20 (1990) 3553; (c) P. Bouyssou, C. Le Goff, J. Chenault, J. Heterocycl. Chem. 29 (1992) 895.
[51] (a) M. Niu, Y. Wang, P. Chen, D. Du, J. Jiang, Z. Jin, Catal, Sci. Technol. 5 (2015) 4746–4749; (b) H.-Y. Jiang, X.-X. Zheng, Appl. Catal. A. 499 (2015) 118–123; (c) H. Mao, X. Liao, B. Shi, Catal. Commun. 16 (2011) 210–214; (d) N.A. Beckers, S. Huynh, X. Zhang, E.J. Luber, J.M. Buriak, ACS Catal. 2 (2012) 1524–1534; (e) M. Campanati, M. Casagrande, I. Fagiolino, M. Lenarda, L. Storaro, M. Battagliarin, A. Vaccari, J. Mol. Catal. A: Chem. 184 (2002) 267–272; (f) C. Bianchini, V.D. Santo, A. Meli, S. Moneti, M. Moreno, W. Oberhauser, R. Psaro, L. Sordelli, F. Vizza, J. Catal. 213 (2003) 47–62; (g) R.-M. Zhang, G.-Y. Fan, C. Li, Y.-Y. Wang, R.-X. Li, H. Chen, X.-J. Li, Acta. Phys. –Chim. Sin. 24 (2008) 965–970; (h) X. Cui, A.-E. Surkus, K. Junge, C. Topf, J. Radnik, C. Kreyenschulte, M. Beller, Nat. Commun. 7 (2016) 11326; (i) B. Sun, D. Carnevale, G. Süss-Fink, J. Org. Chem. 821 (2016) 197–205; (j) H. Mao, C. Chen, X. Liao, B. Shi, J. Mol. Catal. A: Chem. (2011) 51–56.
[52] Y.-P. Sun, H.-Y. Fu, D.-L. Zhang, R.-X. Li, H. Chen, X.-J. Li, Catal. Commun. 12 (2010) 188–192.
[53] G.-Y. Fan, J. Wu, Catal. Commun. 31 (2013) 81–85.
[54] K. Philippot, B. Chaudret, C. R. Chimie 6 (2003) 1019–1034.
[55] T. Pery, K. Pelzer, G. Buntkowsky, K. Philippot, H.-H. Limbach, B. Chaudret, ChemPhysChem. 6 (2005) 605–607.
[56] J. García-Antón, M. Rosa Axet, S. Jansat, K. Philippot, B. Chaudret, T. Pery, G. Buntkowsky, H-H. Limbach, Angew. Chem. 120 (2008) 2104–2108.
[57] F. Novio, K. Philippot, B. Chaudret, Catal. Lett. 140 (2010) 1–7.
[58] J. Ll, P. Castelbou, C. Blondeau, C. Godard Claver, RSC Adv. 5 (2015) 97036–97043.
[59] J. García-Antón, M. Rosa Axet, S. Jansat, K. Philippot, B. Chaudret, T. Pery, G. Buntkowsky, H-H. Limbach, Angew. Chem. Int. Ed. 47 (2008) 2074–2078.
[60] F. Novio, K. Philippot, B. Chaudret, Catal. Lett. 140 (2010) 1–7.
[61] E. Ramirez, L. Eradès, K. Philippot, P. Lecante, B. Chaudret, Adv. Funct. Mater. 17 (2007) 2219–2228.
[62] S.U. Son, Y. Jang, K.Y. Yoon, E. Kang, T. Hyeon, Nano Lett. 4 (2004) 1147–1151.
[63] J.-T. Lu, J.C.Y. Lin, M.-C. Lin, N.D. Khupse, I.J.B. Lin, Langmuir 30 (2014) 10440–10448.
[64] I. Favier, S. Massou, E. Teuma, K. Philippot, B. Chaudret, M. Gómez, Chem. Commun. (2008) 3296–3298.

[65] C. Pan, K. Pelzer, K. Philippot, B. Chaudret, F. Dassenoy, P. Lecante, M.-J. Casanove, J. Am. Chem. Soc. 123 (2001) 7584–7593.
[66] I. Favier, P. Lavedan, S. Massou, E. Teuma, K. Philippot, B. Chaudret, M. Gómez, Top. Catal. 56 (2013) 1253–1261.
[67] J.-T. Lu, J.C.Y. Lin, M.-C. Lin, N.D. Khupse, I.J.B. Lin, Langmuir 30 (2014) 10440–10448.
[68] X.-Y. Yu, B.O. Patrick, B. R. James, Organometallics 25 (2006) 2359–2363.
[69] G.R. Fulmer, A.J.M. Miller, N.H. Sherden, H.E. Gottlieb, A. Nudelman, B.M. Stoltz, J.E. Bercaw, K.I. Goldberg, Organometallics 29 (2010) 2176–2179.
[70] J.D. Scholten, G. Ebeling, J. Dupont, Dalton Trans. (2007) 5554–5560.
[71] F. Novio, D. Monahan, Y. Coppel, G. Antorrena, P. Lecante, K. Philippot, B. Chaudret, Chem. Eur. J. 20 (2014) 1287–1297.
[72] T. Gutmann, I. del Rosal, B. Chaudret, R. Poteau, H.-H. Limbach, G. Buntkowsky, ChemPhysChem 14 (2013) 3026–3033.
[73] L.M. Martinez-Prieto, S. Carenco, C.H. Wu, E. Bonnefille, S. Axnanda, Z. Liu, P.F. Fazzini, K. Philippot, M. Salmeron, B. Chaudret, ACS Catal. 4 (2014) 3160–3168.
[74] T.M. Duncan, K.W. Zilm, D.M. Hamilton, T.W. Root, J. Phys. Chem. 93 (1989) 2583–2590.
[75] A.L. Maksimov, S.N. Kuklin, Y.S. Kardasheva, E.A. Karakhanov, Pet. J. 53 (2013) 157–163.
[76] I.E. Ertas, M. Gulcan, A. Bulut, M. Yurderi, J. Mol. Catal. A.: Chem. 410 (2015) 209–220.
[77] F. Fache, Synlett 15 (2004) 2827–2829.
[78] P. Delbecq, J.-P. Celerier, G. Lhommet, Tetrahedron. Lett. 31 (1990) 4873–4874.
[79] P. Bouyssou, C. Le Goff, J. Chenault, J. Heterocycl. Chem. 29 (1992) 895–898.
[80] R.A. Murphy, A.Y. Chen, S.K. Nair, G.M. Gallego, N.W. Sach, G. Smith, Tetrahedron Lett. (2016) 5588–5591.
[81] H. Plenio, C.M. Thiele, et al., Chem. Eur. J. 14 (2008) 5465–5481.
[82] A.J. Arduengo, R. Krafczyk, R. Schmutzler, Tetrahedron 55 (1999) 14523–14534.
[83] M.D. Fryzuk, W.E. Piers, in: R.B. King, J.J. Eisch (Eds.), in Organometallic Syntheses, Elsevier, Amsterdam, 1986, p. 128.
[84] W. A. Herrmann, in: W.A. Herrmann(Eds.), Synthetic Methods of Organometallic and Inorganic Chemistry, Thieme, Stuttgart, 1996, p. 38.